OCO ray tracing using OCO trajectories

T. A. Coimbra, A. Novais and J. Schleicher – UNICAMP

Abstract

Offset continuation (OCO) is a seismic configuration transform designed to simulate a seismic section as if obtained with a certain source-receiver offset using the data measured with another offset. Since OCO is dependent on the velocity model used in the process, comparison of the simulated section to an acquired section allows for the extraction of velocity information. An algorithm for such a horizon-oriented velocity analysis is based on so-called OCO rays. These OCO rays describe the output point of an OCO as a function of the RMS velocity. The intersection point of an OCO ray with the picked traveltime curve in the acquired data corresponding to the output half-offset defines the RMS velocity at that position. We theoretically relate the OCO rays to the kinematic properties of OCO image waves that describe the continuous transformation of the common-offset reflection event from one offset to another. By applying the method of characteristics to the OCO image-wave equation, we obtain a ray-tracing-like procedure that allows to construct OCO trajectories describing the position of the OCO output point under varying offset. The endpoints of these OCO trajectories for a single input point and different values of the RMS velocity form then the OCO rays. A numerical example demonstrates that the developed ray-tracing procedure leads to reliable OCO rays, which in turn provide high-quality RMS velocities.

Introduction

Operations like dip-moveout correction (DMO), common-shot (CS-)DMO, migration to zero-offset (MZO), azimuth-moveout correction (AMO), as well as shot and offset continuation (SCO and OCO) are important configuration transforms in exploration seismics. The objective of a configuration transform is to simulate a seismic section as if obtained with a certain measurement configuration using the data measured with another configuration. Their applications are manifold, ranging from improved stack, i.e., for data reduction and signal-to-noise enhancement to wave-equation-based trace interpolation to reconstruct missing data and for velocity analysis. The use of configuration transform for these purposes has been demonstrated in a variety of papers, including the following ones on MZO (Bleistein and Cohen, 1995; Tygel et al., 1998), OCO (Fomel and Bleistein, 1996; Santos et al., 1997; Fomel, 2003), SCO (Bagaini and Spagnolini, 1996), AMO (Biondi et al., 1998), DMO (Canning and Gardner, 1996; Collins, 1997), and CS-DMO (Schleicher and Bagaini, 2004).

Any configuration transform can be thought of as being composed of a migration and a subsequent demigration after changing a configuration parameter (Hubral et al., 1996a; Tygel et al., 1996). This points towards their dependence on the velocity model. A first attempt to make use of this velocity dependence was undertaken by Filpo (2005). His idea was to use offset continuation (OCO) for RMS velocity analysis. The objective of an OCO is to transform one common-offset section into another common-offset section with a different offset.

Based on OCO, Filpo (2005) proposed an horizon-based velocity analysis method, where the RMS velocity is determined along some chosen horizons. The input data required are two sets of picked reflection traveltimes for one and the same horizon, but observed in two different common offset sections. Using these data, Filpo (2005) proposes to construct point-to-point OCO maps between the two sets of picks for many different RMS velocities. The resulting variety of output points for a single input point is then called an OCO ray. For each OCO ray, the velocity of the best fit between the mapped and data picks is chosen as the representative of the RMS velocity field of that place. OCO rays are related to the velocity rays as defined by Iversen (2006) and to the concept of image waves as presented by Hubral et al. (1996b).

In this work, we provide a theoretical basis for the OCO rays of Filpo (2005). We start from the OCO eikonal equation of Fomel (1994) and Hubral et al. (1996b). Application of the Method of Characteristics to this partial differential equation leads to a ray theory for the trajectory of a point in the above mentioned map from one offset to another. When fixing the final offset and varying the velocity, the resulting endpoints of these trajectories define an OCO ray in the sense of Filpo (2005).

OCO rays

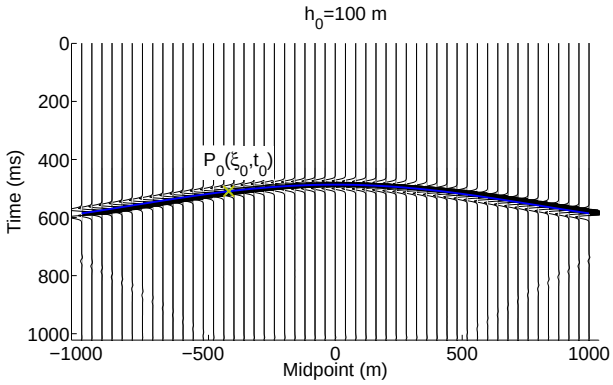

Figure 1: Synthetic common-offset section with $h_0 = 100$ m for a single reflector below a homogeneous overburden. Also shown is the picked arrival time (blue line) and one point $P_0(\xi_0, t_0)$ on it (green cross). These are the input data to offset continuation.

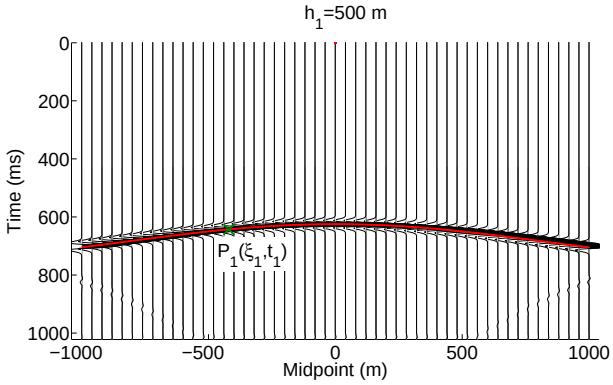

Figure 2: Synthetic common-offset section with $h_1 = 500$ m. Also shown is the OCO map result (red line) including point $P_1(\xi_1, t_1)$, which is the result of the point-to-point OCO map of point P_0.

The concept of OCO rays as introduced by Filpo (2005) can be understood from Figures 1 to 4. These are examples of the OCO ray construction for a single reflector below a homogeneous overburden. Figure 1 shows a synthetic common-offset (CO) section for a small half-offset $h_0 = 100$ m. Also shown is the picked arrival time (blue line) and one point $P_0(\xi_0, t_0)$ on it. An OCO transforms these picks into the corresponding values for a different offset. Figure 2 shows the synthetic CO section for a larger half-offset of $h_1 = 500$ m. Also shown is the OCO result of transforming the picks in Figure 1 to this larger offset (red line). Point $P_1(\xi_1, t_1)$ is the result of the point-to-point OCO map of point P_0. Note the good coincidence of the transform result with the true event.

Of course, this good coincidence is a consequence of having used the true medium velocity. If the velocity used for the OCO map is incorrect, a result like

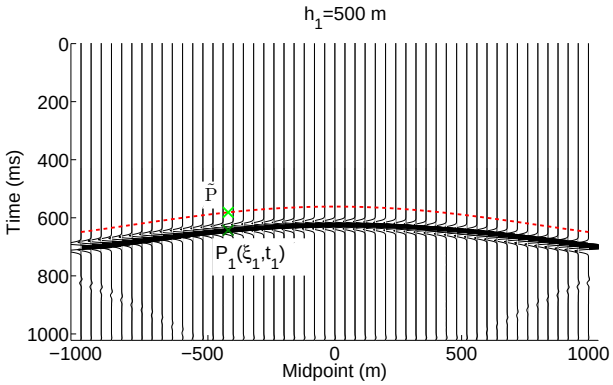

Figure 3: Result of the OCO map when using a wrong velocity (red line). The point P_0 is mapped to a wrong position $\tilde{P}$ (green cross).

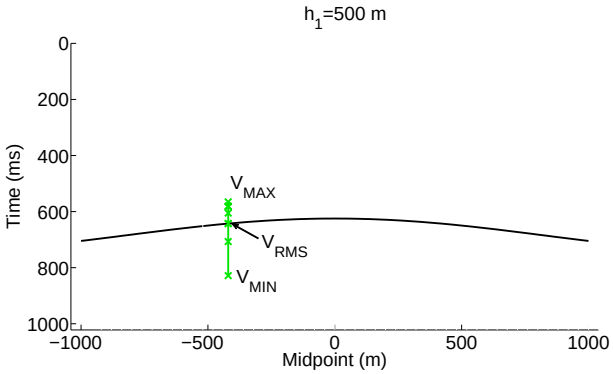

Figure 4: Result of the OCO map when using a set of velocities between $V_{\min}$ and $V_{\max}$. The green line formed by all possible points $\tilde{P}$ crosses the event at the correct velocity.

the one shown in Figure 3 is obtained. The OCO prediction of the reflection traveltime is incorrect and the point P_0 is mapped to a wrong position $\tilde{P}$. This observation brings us to the idea of the OCO ray. When performing the OCO map with a set of possible velocities, varying between $V_{\min}$ and $V_{\max}$, the set of points $\tilde{P}$ will define a trajectory, the so-called OCO ray, which crosses the event in the observed CO section at the correct point P_1 for the correct value of the velocity. In inhomogeneous media, this velocity is the RMS velocity at that position.

A better name for the OCO ray would actually be "OCO velocity ray", reserving the word "OCO ray" for the trajectory that describes the output point of the OCO map as a function of half-offset for a fixed velocity. To avoid confusion, we will refer to this trajectory as the "OCO trajectory".

OCO trajectories

In this work, we develop an analytic procedure to construct the OCO rays. It is based on a ray-tracing-like procedure to construct the OCO maps, i.e., the

set of points P_i for different half-offsets h_i, which we call an OCO trajectory, as a function of velocity. We start from the OCO image-wave equation derived by Fomel (1994) and Hubral et al. (1996b). This OCO image-wave equation is the partial differential equation that describes the change of the primary-reflection image of a subsurface reflector in one CO section to that in another one. It reads

$$ht\left(P_{hh}+\frac{4}{V^2}P_{tt}\right)+\left(t^2+\frac{4h^2}{V^2}\right)P_{ht}-ht\,P_{\xi\xi}=0, \tag{1}$$

where h is half offset, ξ is the midpoint coordinate, t is time, and V is the medium velocity (for the derivation of this equation assumed to be constant). Equation (1) describes an artificial process that transforms the seismic reflection event, $P(\xi,t,h)$, in offset-time domain. Since this transformation is similar to wave propagation, Hubral et al. (1996b) termed it an image wave.

We use the OCO image-wave equation (1) to obtain the trajectory of a single point under this transformation. In other words, we describe the locations of a seismic reflection from the same reflection point in different CO sections.

Since we are only interested in the kinematic description of OCO, we use the ansatz

$$P\left(\xi,t,h\right)=A\left(\xi,t\right)F\left(h-H\left(\xi,t\right)\right) \tag{2}$$

in equation (1). Here, A is the dynamic part, which we are not interested in, F is the wavelet of the reflection event, and H is the image eikonal that represents the kinematic part of the solution. To the leading order, we obtain the image-eikonal equation associated with (1) as

$$\left(1+\frac{4}{V^2}H_t^2\right)tH-\left(t^2+\frac{4}{V^2}H^2\right)H_t-tHH_\xi^2=0. \tag{3}$$

This equation kinematically describes the propagation of OCO image waves.

Method of Characteristics

Equation (3) can be solved using the Method of Characteristics (Courant and Hilbert, 1989). This method will provide us with the characteristic trajectories, along which propagation takes place.

We start by considering the Hamiltonian G given by

$$\begin{aligned}G(\xi,t,H,p,q) &= tH\left(1+\frac{4}{V^2}q^2\right) \\ &\quad -\left(t^2+\frac{4H^2}{V^2}\right)q-tHp^2=0,\end{aligned} \tag{4}$$

where $p=H_\xi$ and $q=H_t$. The method of characteristics consists of transforming equation (4) into the following equation system:

$$\begin{aligned}\frac{d\xi}{dh} &= \lambda G_p=-2\lambda tHp\,,\\ \frac{dt}{dh} &= \lambda G_q=-\frac{\lambda}{V^2}\left(4H^2-8qHt+t^2V^2\right)\,,\\ \frac{dp}{dh} &= \lambda\left(G_pp_\xi+G_qq_\xi\right)=-\lambda\left(G_\xi+pG_h\right)\\ &= -\lambda\left(\frac{p}{V^2}\left(-tp^2V^2+4tq^2-8Hq+tV^2\right)\right)\,,\\ \frac{dq}{dh} &= \lambda\left(G_pp_t+G_qq_t\right)=-\lambda\left(G_t+qG_H\right)\\ &= \frac{\lambda}{2}\Bigg(\frac{1}{V^2}\big(2tp^2qV^2+Hp^2V^2-8tq^3\\ &\quad +12Hq^2-HV^2\big)\Bigg)\,,\\ \frac{dH}{dh} &= \lambda\left(pG_p+qG_q\right)=1\,.\end{aligned} \tag{5}$$

In the first four equations of (5), h could, in principle, be any monotonously increasing variable along the OCO trajectory. For convenience, we have required the independent variable to be the half-offset h. Since on the image wavefront, we have $h=H(\xi,t)$, this requirement leads to the last equation of system (5), which fixes the scaling parameter λ as

$$\lambda=\left(pG_p+qG_q\right)^{-1}=\left(-tHp^2+\frac{4q^2Ht}{V^2}-tH\right)^{-1}. \tag{6}$$

System (5) describes the OCO trajectories as a function of h. In other words, all other variables involved are parameterized as $\xi=\xi(h)$, $t=t(h)$, $p=p(h)$, $q=q(h)$, and $H=H(h)$.

Since the trajectory starts for half-offset h_0 at $P_0(\xi_0,t_0)$, we have the initial values $\xi(h_0)=\xi_0$, $t(h_0)=t_0$ and $H(h_0)=h_0$. From these, we obtain the initial values $p(h_0)=p_0$ and $q(h_0)=q_0$. These values satisfy equation (3) at $h=h_0$, i.e.,

$$t_0h_0\left(1+\frac{4}{V^2}q_0^2\right)-\left(t_0^2+\frac{4h_0^2}{V^2}\right)q_0-t_0h_0p_0^2=0\,, \tag{7}$$

which is equivalent to

$$\left(q_0-A\right)^2-\frac{V^2}{4}p_0^2=B^2\,, \tag{8}$$

where

$$A = \frac{\left(V^2t_0^2+4h_0^2\right)}{8t_0h_0}\,, \tag{9}$$

$$B^2 = A^2-\frac{V^2}{4}>0\,. \tag{10}$$

The fact that B^2 is positive follows from $2A>V$, which in turn is a consequence of $Vt_0>2h_0$.

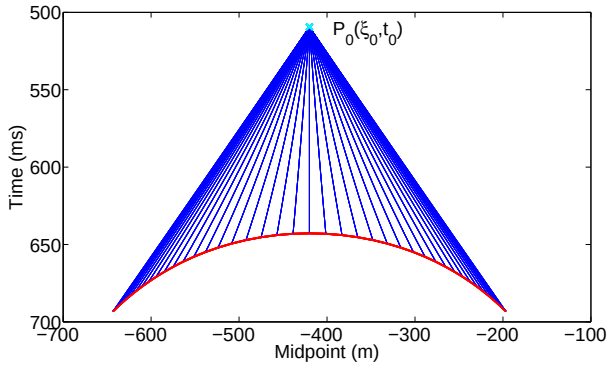

Figure 5: Possible OCO trajectories for a singe point P_0 (blue lines). Indicated in red is the OCO outplanat for P_0, i.e., the surface of all possible points P_1 given by equation (13). In this example, $V = 2500$ m/s, $t_0 = 0.5095$ s, $\xi_0 = -420$ m, $h_0 = 100$ m, and $h_1 = 500$ m.

The solution of equation (8) can be represented as

$$q_0 = B\cosh(\theta) + A\,, \tag{11}$$

$$p_0 = C\sinh(\theta)\,, \qquad \text{with } C = \frac{2B}{V}\,, \tag{12}$$

where θ is a parameter that selects a particular OCO trajectory. Figure 5 shows a set of possible OCO trajectories for the given point P_0. These trajectories were traced with system (5) using initial conditions (11) and (12) with 40 values of θ ranging from -2 to 2. All trajectories end at the OCO outplanat for P_0, i.e., the surface of all possible points P_1 (Santos et al., 1997)

$$t = \tau(\xi_1; P_0) = \frac{2h_1}{V}\sqrt{1 + \frac{V^2 t_0^2 - 4h_0^2}{u^2}}\,, \tag{13}$$

where

$$u = \sqrt{(h_0 + h_1)^2 - \eta^2} + \sqrt{(h_0 - h_1)^2 - \eta^2} \tag{14}$$

and $\eta = \xi_1 - \xi_0$ is the midpoint displacement.

The value of θ that describes the correct OCO trajectory depends on the slope of the traveltime curve at P_0. Denoting this slope by ϕ, we can write

$$\phi = \frac{\partial t}{\partial \xi} = \frac{\partial t}{\partial H}\frac{\partial H}{\partial \xi} = \frac{p_0}{q_0} = \frac{C\sinh(\theta)}{B\cosh(\theta) + A}. \tag{15}$$

Note that $|\phi| < \frac{2}{V}$, i.e., the larger the velocity is, the smaller is the slope of the traveltime curve.

Relationship (15) can be inverted to yield

$$\theta = \ln\left|\frac{2A\phi - \sqrt{V^2\phi^2 + 4C^2}}{C\,(2 - V\phi)}\right|. \tag{16}$$

Here, the negative sign before the square root has been chosen to guarantee that the limit of θ when ϕ tends to $2/V$ is correct.

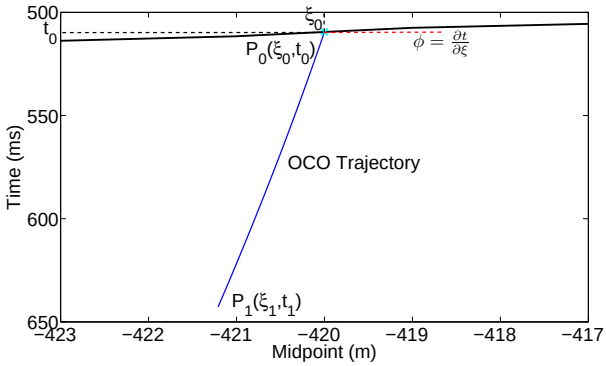

Figure 6: The OCO trajectory for the correct choice of θ according to formula (16).

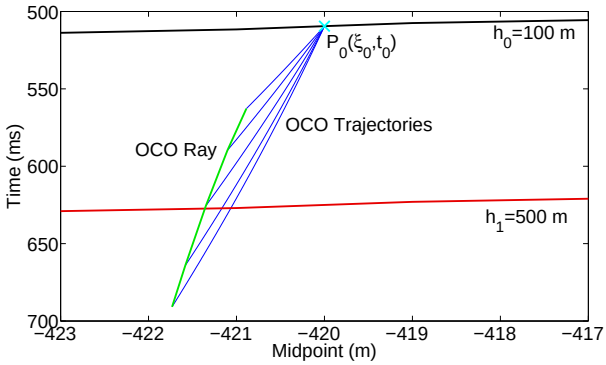

Figure 7: Several OCO trajectories up to $h_1 = 500$ m for different velocities (blue lines). The green line indicates the OCO ray, i.e., the set of all possible OCO map points $\tilde{P}$. Its intersection with the picked traveltime curve for $h_1 = 500$ m (red line) determines the RMS velocity.

From formulas (5), (11), (12), and (16), we recognize that the whole process of tracing OCO trajectories is strongly velocity dependent. Thus, repeating the process with a range of velocity values leads to a set of OCO trajectories. Fixing their final half-offset at the same h_1 yields then the set of all possible position of P_1 as a function of velocity. This set is the OCO ray of Filpo (2005). Figure 7 shows the construction of the OCO ray (green line) using OCO trajectories (blue lines) for the same values of all involved parameters as before. Also shown in Figure 7 is the picked traveltime curve of the reflection event in the CO section with h_1 (red line). The intersection point of the OCO ray with the picked traveltime curve determines the estimate for the RMS velocity.

Numerical example

To demonstrate the velocity extraction procedure using OCO rays, we have employed the technique to synthetic data from the inhomogeneous model of Figure 8. It consists of two constant-velocity layers between two homogeneous halfspaces. The velocities are 1508 m/s, 1581 m/s, 1826 m/s, and 2000 m/s.

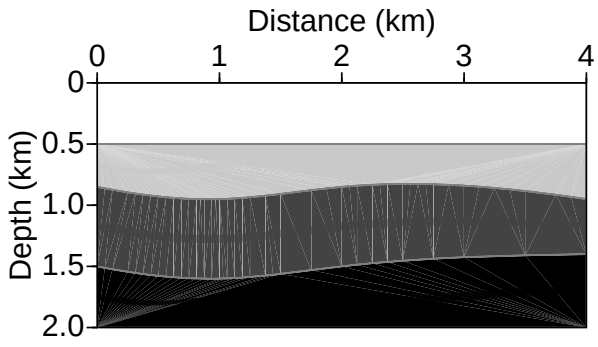

Figure 8: Model for the numerical example.

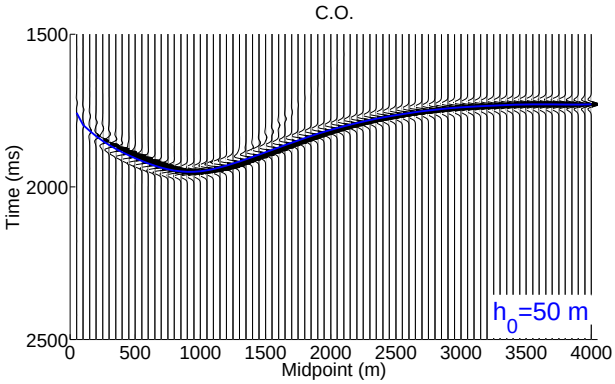

Figure 9: Synthetic CO reflection event with $h_0 = 50$ m of the deepest reflector together with picked reflection traveltime (blue line).

Figure 9 shows the synthetic CO reflection event with $h_0 = 50$ m of the deepest reflector as modeled using Gaussian beams. Also shown is the picked reflection traveltime (blue line).

We used these picks as input to the tracing of the OCO trajectories using system (5). Figure 10 shows the endpoints of all OCO trajectories (red line) obtained using the approximate theoretical value of 1700 m/s for the RMS velocity, superimposed to the synthetic CO section with $h_1 = 250$ m. This demonstrates the high accuracy of the procedure.

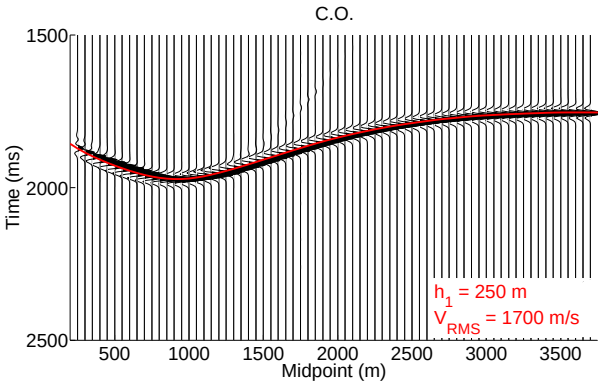

Figure 10: Synthetic CO section with $h_1 = 250$ m, together with the endpoints of all OCO trajectories (red line).

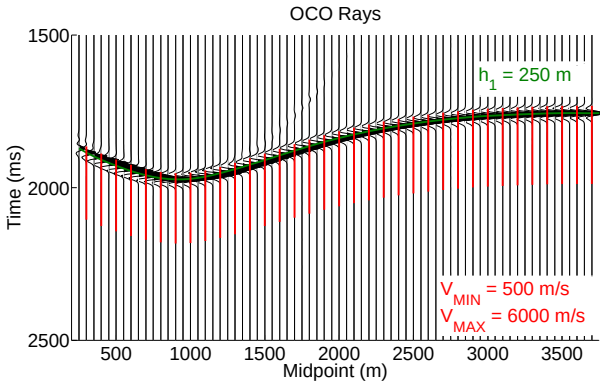

Figure 11: Selected OCO rays (red lines) intersecting the picked traveltime curve (green line) in the output CO section.

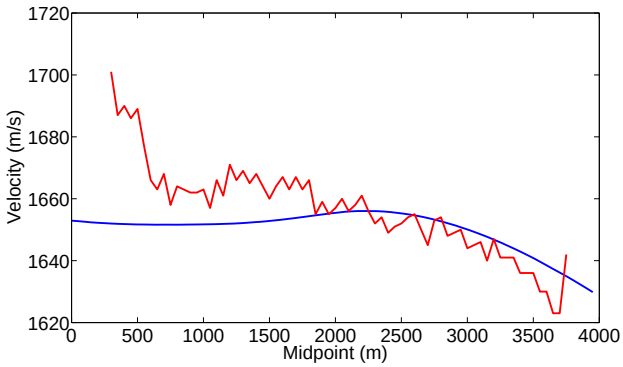

Figure 12: RMS velocity extracted from the intersections of the OCO rays with the picked traveltime in the output CO section (red line) compared to the true RMS velocities for this reflector (blue line).

Next, we tested the RMS velocity extraction using OCO rays. We traced OCO trajectories for each point along the blue line in Figure 9 for a set of velocities between $V_{\min} = 500$ m/s and $V_{\max} = 6000$ m/s. Figure 11 shows a subset of the obtained OCO rays for 20 values of ξ superimposed on the CO section with $h_1 = 250$ m. The intersection points of the OCO rays with the picked event (blue line) determine the extracted RMS velocities. Figure 12 depicts the extracted velocities as a function of ξ and Figure 13 show their relative error. We see that the method is highly reliable with an error in most parts below 1%. The main source of error is the extraction of the traveltime slope ϕ. This was also observed by Pinheiro (2008).

Conclusions

Offset continuation (OCO) is a seismic configuration transform that transforms a seismic common-offset (CO) section for a fixed half-offset into a simulated CO section for another half-offset. The simulated CO section can than be compared with the acquired section for the same half-offset, in this way evaluating the

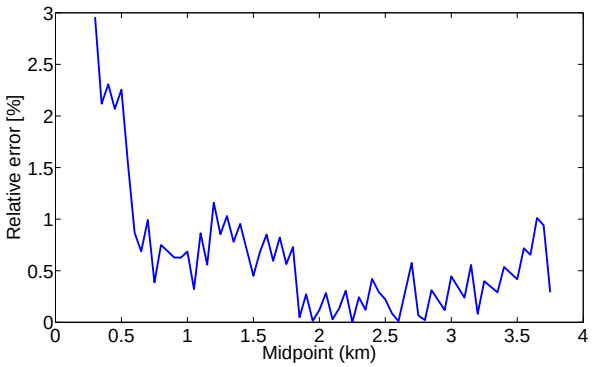

Figure 13: Relative error of extracted RMS velocities.

quality of the velocity field used in the process. If the correct velocity is used, each point on the input reflection traveltime curve is mapped to a point on the output reflection event.

A way to quantify this procedure is based on the OCO rays proposed by Filpo (2005). OCO rays describe the location of the point-to-point maps between the two CO sections as a function of velocity. The intersection point of an OCO ray with the picked traveltime curve in the acquired data corresponding to the output half-offset defines the RMS velocity at that position. In this way, OCO rays allow for the construction of a horizon-based RMS velocity model.

In this work, we have related the OCO rays to image-wave propagation as described by Hubral et al. (1996b). From the kinematic properties of OCO image waves, we have shown how to perform the construction of the OCO maps using a ray-tracing-like procedure, which traces so-called OCO trajectories. An OCO trajectory describes, for a fixed input point, the positions of the OCO output points as a function of output half-offset for a given velocity. The OCO trajectory tracing allows for the construction of the OCO rays of Filpo (2005). Each OCO ray is built up by the endpoints of the set of OCO trajectories for the same input point, input and output half-offsets, but different velocities. A numerical example for a laterally inhomogeneous model demonstrated not only that the so-traced OCO trajectories accurately describe the kinematic properties of the OCO transformation, but also that the OCO rays constructed with the help of OCO trajectories allow to obtain reliable RMS velocities.

Acknowledgments

This work was supported in part by CNPq, FAPESP, CAPES, as well as Petrobras and the sponsors of the Wave Inversion Technology (WIT) Consortium.

References

Bagaini, C. and U. Spagnolini, 1996, 2D continuation operators and their applications: Geophysics, **61**, 1846–1858.

Biondi, B., S. Fomel, and N. Chemingui, 1998, Azimuth moveout for 3-D prestack imaging: Geophysics, **63**, 574–588.

Bleistein, N. and J. Cohen, 1995, The effect of curvature on true-amplitude DMO: Proof of concept: Research Note, Center for Wave Phenomena, **CWP-193**.

Canning, A. and G. H. F. Gardner, 1996, Regularizing 3D data sets with DMO: Geophysics, **61**, 1101–1114.

Collins, C. L., 1997, Imaging in 3D DMO; Part I: Geometrical optics model; Part II: Amplitude effects: Geophysics, **61**, 211–244.

Courant, R. and D. Hilbert, 1989, Methods of mathematical physics: John Wiley & Sons.

Filpo, E., 2005, Horizon velocity analysis using OCO rays: 9th 9th Internat. Congress, SBGf, Expanded Abstracts, SBGf372:1–4.

Fomel, S., 2003, Theory of differential offset continuation: Geophysics, **68**, 718–732.

Fomel, S. and N. Bleistein, 1996, Amplitude preservation for offset continuation: Confirmation for Kirchhoff data: Technical Report CWP, Colorado School of Mines, **CWP-197**.

Fomel, S. B., 1994, Kinematically equivalent differential operators for offset continuation of seismic sections: Russian Geology and Geophysics, **35**, no. 9, 146–160.

Hubral, P., J. Schleicher, and M. Tygel, 1996a, A unified approach to 3-D seismic reflection imaging – Part I: Basic concepts: Geophysics, **61**, 742–758.

Hubral, P., M. Tygel, and J. Schleicher, 1996b, Seismic image waves: Geophysical Journal International, **125**, 431–442.

Iversen, E., 2006, Velocity rays for heterogeneous anisotropic media: Theory and implementation: Geophysics, **71**, T117–T127.

Pinheiro, L., 2008, Construção de modelos de velocidade utilizando critérios de consistência: PhD thesis, Universidade Federal do Rio de Janeiro.

Santos, L., J. Schleicher, and M. Tygel, 1997, 2.5-D true-amplitude offset continuation: J. Seism. Expl., **6**, 103–116.

Schleicher, J. and C. Bagaini, 2004, Controlling amplitudes in 2.5D common-shot migration to zero offset: Geophysics, **69**, 1299–1310.

Tygel, M., J. Schleicher, and P. Hubral, 1996, A unified approach to 3-D seismic reflection imaging – Part II: Theory: Geophysics, **61**, 759–775.

Tygel, M., J. Schleicher, P. Hubral, and L. Santos, 1998, 2.5-D true-amplitude Kirchhoff migration to zero offset in laterally inhomogeneous media: Geophysics, **63**, 557–573.